

Fermi surface and effective masses in photoemission response of the $(\text{Ba}_{1-x}\text{K}_x)\text{Fe}_2\text{As}_2$ superconductor

Gerald Derondeau,^{1,*} Federico Bisti,² Jürgen Braun,¹ Victor A. Rogalev,² Masaki Kobayashi,^{2,3} Ming Shi,² Thorsten Schmitt,² Junzhang Ma,^{2,4,5} Hong Ding,^{4,5} Hubert Ebert,¹ Vladimir N. Strocov,^{2,†} and Ján Minár^{1,6,‡}

¹*Department Chemie, Physikalische Chemie, Universität München, Butenandtstr. 5-13, 81377 München, Germany*

²*Swiss Light Source, Paul Scherrer Institute, CH-5232 Villigen PSI, Switzerland*

³*Department of Applied Chemistry, School of Engineering, University of Tokyo, 7-3-1 Hongo, Bunkyo-ku, Tokyo 113-8656, Japan*

⁴*Beijing National Laboratory for Condensed Matter Physics*

⁵*Institute of Physics, Chinese Academy of Sciences, Beijing 100190, China*

⁶*New Technologies-Research Center, University of West Bohemia, Pilsen, Czech Republic*

(Dated: June 26, 2022)

The angle-resolved photoemission spectra of the superconductor $(\text{Ba}_{1-x}\text{K}_x)\text{Fe}_2\text{As}_2$ have been investigated both experimentally and theoretically. Our results explain the previously obscured origins of all salient features of the ARPES response of this paradigm pnictide compound and reveal the origin of the Lifshitz transition. Comparison of calculated ARPES spectra with the underlying DMFT band structure shows an important impact of final state effects, which results for three-dimensional states in a deviation of the ARPES spectra from the true spectral function. In particular, the apparent effective mass enhancement seen in the ARPES response is not an entirely intrinsic property of the quasiparticle valence bands but may have a significant extrinsic contribution from the photoemission process and thus differ from its true value. Because this effect is more pronounced for low photoexcitation energies, soft-X-ray ARPES delivers more accurate values of the mass enhancement due to a sharp definition of the 3D electron momentum.

The iron pnictides are nowadays one of the most studied examples for unconventional superconductivity. Due to their complex properties standard theoretical methods based on a local density approximation (LDA) within density functional theory (DFT) often fail.[1–3] This is especially true if one tries to explain angle-resolved photoemission (ARPES) spectra of the iron pnictides.[4–11] In this context a significant discrepancy between the effective masses derived from experimental ARPES spectra m_{exp}^* and from LDA band structure calculations m_{LDA}^* was reported.[9, 11] Correct trends in the effective masses can be observed using dynamical mean-field theory (DMFT) approaches which quantifies the importance of correlation effects for the iron pnictides.[12, 13]

Various advanced approaches have been applied in the field, accounting for different phenomena. This covers the treatment of disorder in an appropriate way [14–16], the inclusion of spin-orbit coupling (SOC) [17] and in order to calculate ARPES spectra correctly the influence of matrix element effects and surface effects was recently stressed [18, 19]. Finally, electron-electron correlation effects are one of the most important issues discussed.[8, 12, 20–24] All these aspects were shown to play a crucial role for the iron pnictides, yet most approaches so far can deal with only one of these issues at the same time.

In this work we will present a theoretical approach which accounts for all of the above mentioned issues leading in this way to a very satisfactory agreement with experimental ARPES data of the iron pnictides. Here we investigate one of the most prominent prototype systems in the family of iron pnictides, namely the K

substituted $(\text{Ba}_{1-x}\text{K}_x)\text{Fe}_2\text{As}_2$ compound [25, 26], which was extensively studied by ARPES.[4–7, 10, 27, 28] There is common agreement, that the Fermi surface (FS) of this compound is quite complex and cannot be obtained from plain DFT calculations. In fact, an exceptional propeller-like FS topology at the \bar{X} point is found [4–6] which is discussed in terms of a Lifshitz transition, meaning topological changes in the FS which mark the onset of superconductivity.[16, 29] Also a rather puzzling change in the intensity distribution at neighboring $\bar{\Gamma}$ points is known.[4] Until now there is no theoretical work which would explain all the salient features of the ARPES spectra of $(\text{Ba}_{1-x}\text{K}_x)\text{Fe}_2\text{As}_2$.

Results

Impact of correlations on the electronic structure.

The crystal structure of $(\text{Ba}_{0.6}\text{K}_{0.4})\text{Fe}_2\text{As}_2$ is shown in Fig. 1 (A), with the corresponding Brillouin zone (BZ) and its two-dimensional counterpart for a (001) orientated surface given in Fig. 1 (B). The electronic structure is represented by means of the Bloch spectral function (BSF), which has the significant advantage that in the presented approach all disorder effects induced through substitution are fully accounted for. The LDA based band structure is shown in Fig. 1 (C) with the corresponding Fermi surface (FS) cut shown in Fig. 1 (D). The topology of this FS cut fails to explain the Fermi surface seen by ARPES.[4] It can neither reproduce the well-known propeller-like features at the \bar{X} point, nor it can explain the flower-like topology at $\bar{\Gamma}'$. [4] Thus, the applied LDA approach is insufficient to deal accurately

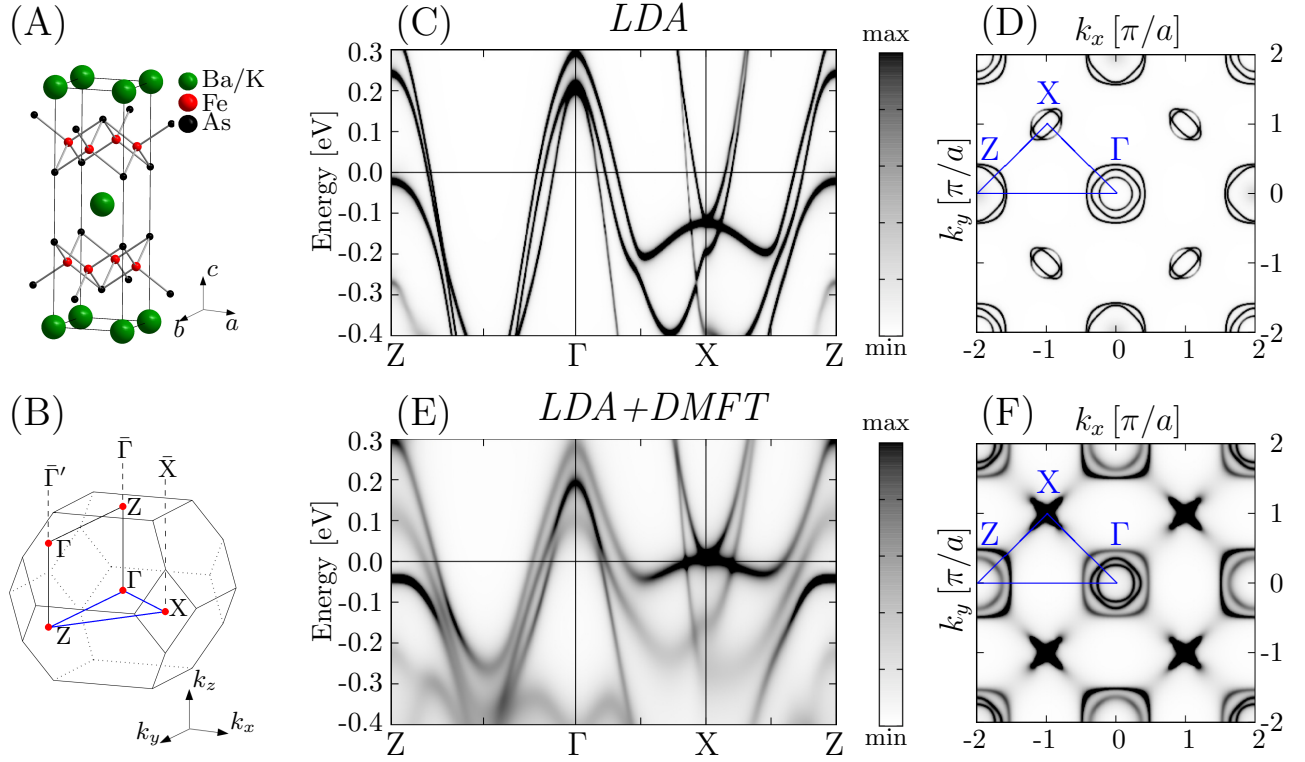


FIG. 1. (A) Crystallographic unit cell of tetragonal $(\text{Ba}_{1-x}\text{K}_x)\text{Fe}_2\text{As}_2$ with (B) corresponding Brillouin zones indicating the important high symmetric points. $\bar{\Gamma}$, $\bar{\Gamma}'$ and \bar{X} indicate the two-dimensional Brillouin zone for a (001) orientated surface. (C + D) BSF and FS of $(\text{Ba}_{0.6}\text{K}_{0.4})\text{Fe}_2\text{As}_2$ calculated on the basis of LDA. (E + F) Corresponding BSF and FS of $(\text{Ba}_{0.6}\text{K}_{0.4})\text{Fe}_2\text{As}_2$ calculated on the basis of LDA+DMFT. The blue lines always indicate the path chosen for the presented band structure.

with these prominent features. To account for the necessary correlation effects fully self-consistently, we have applied subsequent LDA+DMFT calculations. We used for Fe an averaged on-site Coulomb interaction $U = 3.0$ eV and an exchange interaction $J = 0.9$ eV, which are commonly used for the iron pnictides.[8, 30, 31] The impact of correlation effects represented by the DMFT on the band structure in Fig. 1 (E) and on the Fermi surface cut in Fig. 1 (F) is tremendous. We see strong renormalization of the d_{xy} and $d_{xz/yz}$ bands, in agreement with other literature.[13] However, most prominent are the changes around the X point where a significant upwards shift of the bands towards the Fermi level (E_F) leads to the hole and electron pockets responsible for the appearance of the propeller like topology at \bar{X} in agreement with experimental ARPES data.[4–6] Note, that a similar upwards shift at X of around 0.1 eV was also observed by Werner *et al.*[8] [32], although the qualitative agreement of our results with experiment seems slightly better. In comparison, Werner *et al.* used a frequency dependent screening which leads to strong incoherence. However, based on suggestions by Tomczak *et al.*[12] and because we look only at energies close to the Fermi level it seems like an acceptable approximation to use a static coulomb interaction U . In particular, we are able to fully account for the chemical disorder of the K-doped com-

pound in terms of the coherent potential approximation (CPA) which seems to be more relevant for the problem at hand. Considering the LDA band structure from Fig. 1 (C) one can already see strong band broadening for the hole band of interest at X. Thus, incoherence due to disorder effects is strongest for explicitly this band and it would be invalid to neglect this. Consequently, strong incoherence at X for the LDA+DMFT band structure makes it difficult to resolve the exact band shape. Based on the ARPES data of Zabolotnyy *et al.*[4] the electron pocket and the hole pocket at X should hybridize even more than in the presented calculations. This effect is covered in our results due to the strong incoherence and it might be also a shortcoming of the applied FLEX DMFT solver.

Still, the consequence of this phenomenon is a topological change in the FS contour, indicating a so-called Lifshitz transition which is crucial for the emergence of superconductivity.[16, 29] This Lifshitz transition was already discussed for high K concentrations ($x \approx 0.9$) within a LDA framework.[16, 28] The present as well as previous experimental work [4–6], however, clearly shows the emergence of the petal topology around \bar{X} already for optimal doping ($x \approx 0.4$). Based on the latter discussion and by comparing Fig. 1 (C) and (D) one can see that the origin of the Lifshitz transition at

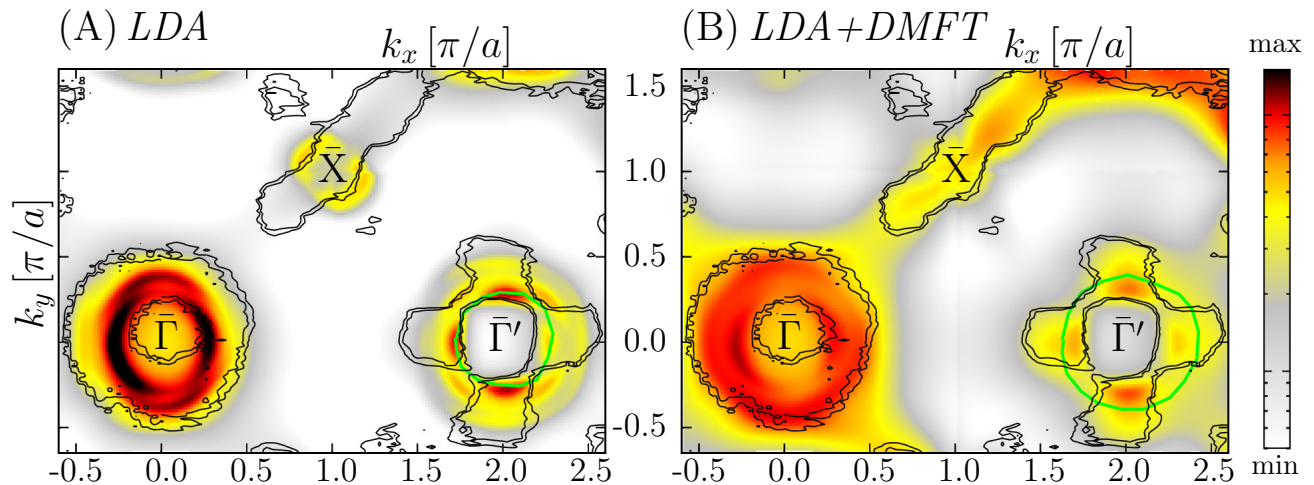


FIG. 2. Fermi surfaces cuts of $(\text{Ba}_{0.6}\text{K}_{0.4})\text{Fe}_2\text{As}_2$ for $h\nu = 75$ eV as seen by one step model ARPES calculations for (A) LDA and (B) LDA+DMFT. The overlay of black isolines always corresponds to experimental ARPES data taken with permission from Zabolotnyy *et al.* [4]. The green solid lines are guides for the eyes to indicate surface state related features.

lower K concentrations is fully controlled by correlation effects accounted for by the applied LDA+DMFT approach. Consequently, the Lifshitz transition can also qualitatively explain the breakdown of magnetic order for $(\text{Ba}_{1-x}\text{K}_x)\text{Fe}_2\text{As}_2$, which takes place at low doping ratios $x < 0.4$ [26], as it destroys the nesting condition [33]. More details showing the clear dependence on the Coulomb interaction U are found in the Supplemental Material [34]. Although, the applied self-consistent DMFT approach has brought important new insights on the topology around \bar{X} , it is not able to reproduce the flower-like intensity distribution observed at $\bar{\Gamma}'$ compared to $\bar{\Gamma}$. [4]

Impact of ARPES response effects. To understand this flower-like feature, additional calculations based on the one-step model of ARPES have been done, accounting for the experimental geometry [35, 36] including surface effects as well as matrix element effects. These calculations were performed using the LDA potentials and within the LDA+DMFT framework. The corresponding spectroscopic Fermi surface cuts obtained from the one-step model ARPES calculations of $(\text{Ba}_{0.6}\text{K}_{0.4})\text{Fe}_2\text{As}_2$ for $h\nu = 75$ eV are shown in Fig. 2 (A) for LDA and in Fig. 2 (B) for the LDA+DMFT calculations. For comparison we show in both pictures the original experimental data from Zabolotnyy *et al.* [4] as an overlay of black isolines, measured at $h\nu = 80$ eV.

The ARPES calculations based on the LDA+DMFT shown in Fig. 2 (B) reveal very good agreement with the experimental data, concerning the Lifshitz transition induced propeller structure at \bar{X} (only one part of the propeller is clearly visible for the chosen light polarization as was also found in experiment [4]) indicating that the previously discussed electronic structure is correctly reproduced. Furthermore, we obtain good agreement con-

cerning the flower intensity distribution at $\bar{\Gamma}'$. It should be stressed that there is no alternation of this circle and flower topology around $\bar{\Gamma}$ and $\bar{\Gamma}'$, respectively, with alternating Γ and Z points in the k_z direction by changing $h\nu$. Thus, the origin of this interesting topology is not connected to the alternation between Γ and Z points of the bulk Brillouin zone.

The general appearance of two different shapes between $\bar{\Gamma}$ and $\bar{\Gamma}'$ can be explained by the structure factor and the light polarization in terms of a 1-Fe or 2-Fe cell, as discussed by e.g. Moreschini *et al.* [37] or Lin *et al.* [38]. Note, that a correct treatment of the phase difference between two atoms of a unit cell and the light polarization is by construction included in the one-step model of photoemission (see Ref. [39]), thus the theory can sufficiently account for this. However, we find that at the same time other effects can contribute, in order to obtain this flower topology in agreement with experiment. As can be seen from Fig. 2 (A) the intensity distribution at $\bar{\Gamma}'$ has a fourfold rotational symmetry, although the flower-like topology is not adequately reproduced compared to the result in Fig. 2 (B). This difference cannot be explained without additional contributions.

It is known that the intensity distributions in ARPES might change for neighboring Brillouin zones between $\bar{\Gamma}$ and $\bar{\Gamma}'$ due to matrix element effects, however, such a strong change in the intensity distribution as seen in experiment [4] and reproduced in Fig. 2 (B) is rather uncommon and unexpected. Yet, it is also known that the influence of matrix element effects can be enhanced in the vicinity of surface related states. Surface phenomena can be investigated by the applied method, as it is explained in more detail in Ref. [40]. In particular, we have recently shown that surface states have a significant influence on the ARPES spectra of Co-doped BaFe_2As_2 [19]. Subsequently, one is able to identify

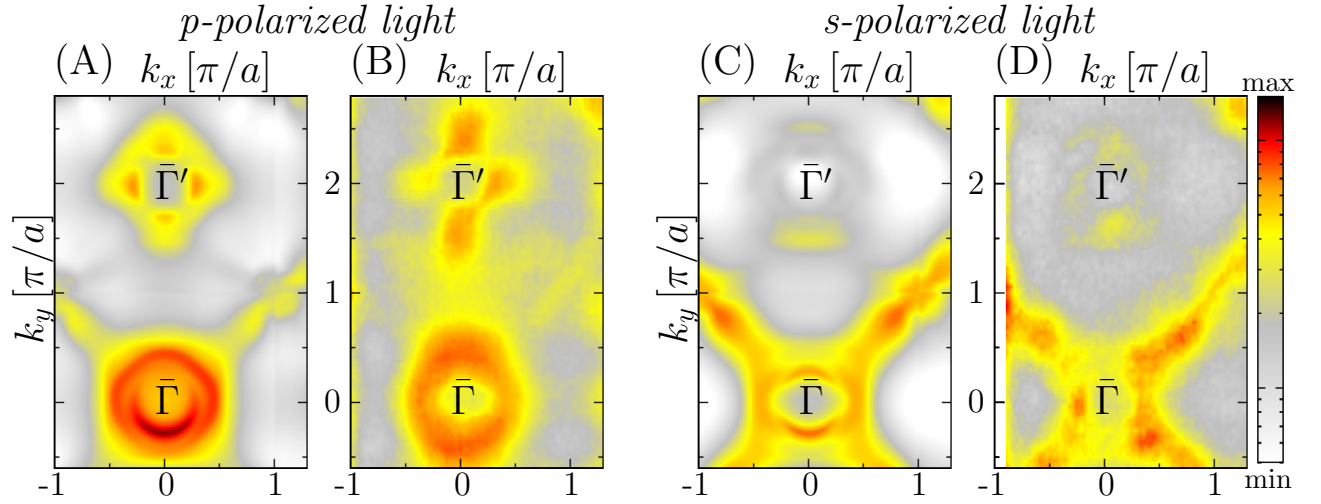


FIG. 3. Fermi surface cuts of $(\text{Ba}_{0.6}\text{K}_{0.4})\text{Fe}_2\text{As}_2$ for (A+C) $h\nu = 425$ eV ARPES calculation using LDA+DMFT and (B+D) $h\nu = 430$ eV experimental data. The incoming light was either (A+B) p -polarized or (C+D) s -polarized.

in the spectra of $(\text{Ba}_{0.6}\text{K}_{0.4})\text{Fe}_2\text{As}_2$ surface resonance states which wave functions have bulk Bloch asymptotic behavior and exhibit a strong resonance at the vicinity of the surface. This means such surface resonances can show a k_z dispersion and they can be observed also for comparably high photon energies. The positions of these ring-shaped surface resonances is marked with solid green lines as an overlay in Fig. 2. For LDA in Fig. 2 (A) one can see that this surface resonance is compressed and thus its influence on the intensity distribution at $\bar{\Gamma}'$ is less significant. In comparison, the surface resonance is shifted for the LDA+DMFT calculation in Fig. 2 (B) where it cuts precisely through the clearly visible petals of the flower topology, affecting the intensity distribution at this position. We believe, that these contributions from the surface resonances can

add up to the commonly discussed explanation based on the 1-Fe/2-Fe scheme, giving finally an overall good agreement with experimental data.

New bulk sensitive ARPES experiments. Additional bulk sensitive soft-X-ray photoemission measurements for $h\nu = 430$ eV were performed for samples of $(\text{Ba}_{0.6}\text{K}_{0.4})\text{Fe}_2\text{As}_2$. The resulting spectra are presented in Figs. 3 (B) and (D) for p -polarized and s -polarized light, respectively. Notably, for p -polarized light the flower shaped topology at $\bar{\Gamma}'$ is enhanced in intensity while for s -polarized light the propeller topologies at \bar{X} are enhanced. Corresponding calculations for $h\nu = 425$ eV are presented in Figs. 3 (A) and (C), which show very good agreement with the experimental data concerning the relevant topologies and the polarization dependence. Thus, these experiments are fully in line with the argumentation of this work so far and further validate our results. Additional extended Fermi surface cuts for higher Brillouin zones can be found in the Supplemental Material.[34]

Furthermore, the experimental k_z scan from 350 eV up to 500 eV is shown in Fig. 4 with the photon energy of $h\nu = 430$ eV explicitly marked with the black line. This shows clearly the k_z dispersion and thus the strong 3D character of the iron pnictides.

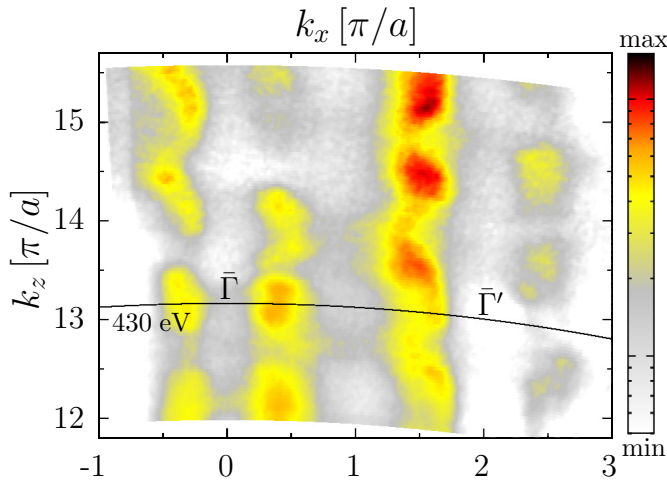


FIG. 4. Experimental k_z scan with p -polarized light for $(\text{Ba}_{0.6}\text{K}_{0.4})\text{Fe}_2\text{As}_2$ from 350 eV up to 500 eV. It is showing the clear k_z dispersion at $\bar{\Gamma}$ and $\bar{\Gamma}'$. The photon energy of $h\nu = 430$ eV is marked with a black line.

Effective masses derived from ARPES spectra Finally, the electronic structure derived from BSF calculations and ARPES calculations was used to analyze the effective masses which are of great actual interest for the iron pnictides.[9, 11–13] The results for the mass ratios of the inner and outer hole pockets around Γ in the ΓZ direction and additionally for the hole pocket at X in the ΓX direction are summarized in Tab. I. More details are found in the Supplemental Material.[34] As

TABLE I. Ratio of effective masses of m_{DMFT}^* to m_{LDA}^* for the Bloch spectral function (BSF) calculations as well as for the ARPES calculations with $h\nu = 75$ eV and 425 eV, respectively. The values correspond to the inner and outer hole pockets around Γ showing strong k_z dispersion and to the hole pocket at X showing weak k_z dispersion.[34]

$\frac{m_{\text{DMFT}}^*}{m_{\text{LDA}}^*}$	BSF	ARPES 75 eV	ARPES 425 eV
Inner pocket Γ	2.59	3.66	2.94
Outer pocket Γ	1.70	2.28	1.98
Hole pocket X	1.43	1.56	1.58

it is commonly done, all values of m^* are normalized to the LDA value m_{LDA}^* deduced from the ground state BSF. First, consider the mass enhancement at Γ only, where the influence of DMFT on the band dispersion can be seen for the BSF, with an average mass enhancement of 2.15 (meaning an average over inner and outer hole pocket Γ), being in good agreement with literature (e.g. 2.04 for KFe_2As_2 [13]). Of more interest is the apparent mass enhancement deduced from the ARPES calculations compared to the BSF band dispersion. The difference is attributed to the fact that the calculated ARPES spectra include not only the correlation effects of DMFT but also final state effects which, as explained below, modify the ARPES spectral shape. On the experimental side, such an apparent mass enhancement has already been observed in ARPES for e.g. the BaFe_2As_2 parent compound and connected with the k_z dispersion of the valence states.[9] The apparent mass enhancement is given by the fact that the ARPES response of the 3D valence states is formed by averaging of their matrix-element weighted k_z dispersion over an interval of the intrinsic final state k_z broadening (Δk_z) determined by the photoelectron mean free path λ . [41, 42] As illustrated in Fig. S5 in the Supplemental Material [34], near the extremes of the valence band k_z dispersions this averaging effectively shifts the ARPES peaks from true k_z dispersions into the band interior (for detailed physical picture see Ref. [41]). In k_{\parallel} dependent ARPES intensities this shift is seen as an apparent bandwidth reduction and corresponding mass enhancement. One can expect a stronger influence of these final state effects at lower photon energies where Δk_z is larger due to a smaller λ . Indeed, our calculations find significant differences in the mass enhancement at Γ depending on $h\nu$. For the low $h\nu$ of 75 eV ($\Delta k_z = 0.2779 \text{ \AA}^{-1}$, which makes about 30% of the perpendicular BZ dimension) we find an average mass enhancement of 2.97 at Γ which is higher than the value of 2.15 obtained from the BSF. The significantly higher $h\nu$ of 425 eV ($\Delta k_z = 0.1228 \text{ \AA}^{-1}$) increases λ and concomitantly improves the k_z definition. The final state effects have therefore a less pronounced contribution, reducing the average mass enhancement at Γ to 2.46. This is true for

almost all bands in the iron pnictides as they are 3D materials with most bands showing a clear k_z dispersion. One of the rare exceptions for the $(\text{Ba}_{1-x}\text{K}_x)\text{Fe}_2\text{As}_2$ compound is the hole pocket at X which has almost 2D character and shows hardly a k_z dispersion as can be seen in Fig. 1 (C + E) for the path ΓXZ . In such a case one would expect significantly less influence of the final-state effects and indeed, Tab. I shows that the apparent mass enhancement for high and low $h\nu$ at X is almost the same and very similar to the BSF mass enhancement. This finally explains discrepancies in the observed mass enhancement for the iron pnictides. To reduce these $h\nu$ dependent deviations of the ARPES response from the true 3D valence bands, we justify the use of higher $h\nu$ in the soft-X-ray regime to improve the k_z definition.

Discussion

In conclusion, the presented LDA+DMFT+ARPES study is the first to quantitatively match theoretical description and experimental ARPES data on the paradigm high-temperature superconductor $(\text{Ba}_{0.6}\text{K}_{0.4})\text{Fe}_2\text{As}_2$. These results enable better physical understanding of the unconventional superconductivity in pnictides and will be of great importance for future studies on similar systems. In particular, the origin of the Lifshitz transition in $(\text{Ba}_{1-x}\text{K}_x)\text{Fe}_2\text{As}_2$, crucial for its superconductivity, is identified as fully controlled by electron correlation effects, which we have discussed in detail. Furthermore, we have shown that due to the inherently 3D nature of the iron pnictides their ARPES response is significantly influenced by final state effects, shifting the spectral peaks from the true quasiparticle valence bands. Their mass enhancement apparent in the ARPES spectra is then different from the true value and, moreover, will depend on the photon energy. Thus, the mass renormalization observed in previous ARPES works on iron pnictides is not an entirely intrinsic property of the quasiparticle valence band structure or spectral function, but has a significant contribution due to a peculiarity of the photoemission process extrinsic to the true valence band properties.

Methods

Computational method. Within the present work, the multiple scattering Korringa-Kohn-Rostoker-Green function (KKR-GF) method was applied which allows to deal simultaneously with all mentioned spectroscopic and many-body aspects. All calculations have been performed within the fully relativistic four component Dirac formalism [43, 44], accounting this way for all effects induced by spin-orbit coupling. Disorder effects are dealt with by means of the coherent potential approximation (CPA).[16, 19, 45] ARPES calculations are based on the one-step model of photoemission in its spin density matrix formulation using the experimental

geometry.[46, 47] Thus, the theory accounts for effects induced by the light polarization, matrix-element effects, final state effects and surface effects. To account for correlation effects fully self-consistently (concerning charge as well as self energy) the LDA+DMFT method using a FLEX solver was applied.[48] For Fe an averaged on-site Coulomb interaction $U = 3.0$ eV and an exchange interaction $J = 0.9$ eV were applied. In the Supplemental Material calculations for different values of U are shown.[34] The lattice constants of the tetragonal cell of $(\text{Ba}_{0.6}\text{K}_{0.4})\text{Fe}_2\text{As}_2$ were taken from experimental data.[26]

ARPES experiments. New ARPES experiments in the soft-X-ray photon energy ($h\nu$) range above 400 eV were performed at the ADRESS beamline of the Swiss Light Source synchrotron facility.[35, 36] By using higher $h\nu$ compared to the conventional ultraviolet ARPES, higher bulk sensitivity is achieved due to an increase of the photoelectron mean free path λ as expected from the well-known “universal curve”. Crucial for 3D materials like the iron pnictides is that the increase of λ results, by the Heisenberg uncertainty principle, in a sharp intrinsic definition of the momentum k_z perpendicular to the surface.[41] As explained in the paper, the latter becomes important for the correct evaluation of the true valence band dispersions and effective masses.

In particular, bulk sensitive soft-X-ray photoemission measurements for $h\nu = 430$ eV were performed for in-situ cleaved samples of $(\text{Ba}_{0.6}\text{K}_{0.4})\text{Fe}_2\text{As}_2$ at a temperature of around 12 K and with an overall energy resolution of around 70 meV.

References

- * gerald.derondeau@cup.uni-muenchen.de
- † vladimir.strocov@psi.ch
- ‡ jan.minar@cup.uni-muenchen.de
- [1] I. I. Mazin and M. D. Johannes, *Nature Physics* **5**, 141 (2009).
- [2] I. I. Mazin, D. J. Singh, M. D. Johannes, and M. H. Du, *Phys. Rev. Lett.* **101**, 057003 (2008).
- [3] I. I. Mazin, M. D. Johannes, L. Boeri, K. Koepernik, and D. J. Singh, *Phys. Rev. B* **78**, 085104 (2008).
- [4] V. B. Zabolotnyy, D. S. Inosov, D. V. Evtushinsky, A. Koitzsch, A. A. Kordyuk, G. L. Sun, J. T. Park, D. Haug, V. Hinkov, A. V. Boris, C. T. Lin, M. Knupfer, A. N. Yaresko, B. Büchner, A. Varykhalov, R. Follath, and S. V. Borisenko, *Nature* **457**, 569 (2009).
- [5] D. V. Evtushinsky, D. S. Inosov, V. B. Zabolotnyy, M. S. Viazovska, R. Khasanov, A. Amato, H.-H. Klauss, H. Luetkens, C. Niedermayer, G. L. Sun, V. Hinkov, C. T. Lin, A. Varykhalov, A. Koitzsch, M. Knupfer, B. Büchner, A. A. Kordyuk, and S. V. Borisenko, *New Journal of Physics* **11**, 055069 (2009).
- [6] D. V. Evtushinsky, A. A. Kordyuk, V. B. Zabolotnyy, D. S. Inosov, T. K. Kim, B. Büchner, H. Luo, Z. Wang, H.-H. Wen, G. Sun, C. Lin, and S. V. Borisenko, *J. Phys. Soc. Japan* **80**, 023710 (2011).
- [7] D. V. Evtushinsky, D. S. Inosov, V. B. Zabolotnyy, A. Koitzsch, M. Knupfer, B. Büchner, M. S. Viazovska, G. L. Sun, V. Hinkov, A. V. Boris, C. T. Lin, B. Keimer, A. Varykhalov, A. A. Kordyuk, and S. V. Borisenko, *Phys. Rev. B* **79**, 054517 (2009).
- [8] P. Werner, M. Casula, T. Miyake, F. Aryasetiawan, A. J. Millis, and S. Biermann, *Nature Physics* **8**, 331 (2012).
- [9] V. Brouet, P.-H. Lin, Y. Texier, J. Bobroff, A. Taleb-Ibrahimi, P. Le Fèvre, F. Bertran, M. Casula, P. Werner, S. Biermann, F. Rullier-Albenque, A. Forget, and D. Colson, *Phys. Rev. Lett.* **110**, 167002 (2013).
- [10] D. V. Evtushinsky, V. B. Zabolotnyy, T. K. Kim, A. A. Kordyuk, A. N. Yaresko, J. Maletz, S. Aswartham, S. Wurmehl, A. V. Boris, D. L. Sun, C. T. Lin, B. Shen, H. H. Wen, A. Varykhalov, R. Follath, B. Büchner, and S. V. Borisenko, *Phys. Rev. B* **89**, 064514 (2014).
- [11] V. Brouet, D. LeBoeuf, P.-H. Lin, J. Mansart, A. Taleb-Ibrahimi, P. Le Fèvre, F. Bertran, A. Forget, and D. Colson, *Phys. Rev. B* **93**, 085137 (2016).
- [12] J. M. Tomczak, M. van Schilfgaarde, and G. Kotliar, *Phys. Rev. Lett.* **109**, 237010 (2012).
- [13] S. Backes, D. Guterding, H. O. Jeschke, and R. Valentí, *New Journal of Physics* **16**, 083025 (2014).
- [14] T. Berlijn, C.-H. Lin, W. Garber, and W. Ku, *Phys. Rev. Lett.* **108**, 207003 (2012).
- [15] L. Wang, T. Berlijn, Y. Wang, C.-H. Lin, P. J. Hirschfeld, and W. Ku, *Phys. Rev. Lett.* **110**, 037001 (2013).
- [16] S. N. Khan and D. D. Johnson, *Phys. Rev. Lett.* **112**, 156401 (2014).
- [17] S. V. Borisenko, D. V. Evtushinsky, Z.-H. Liu, I. Morozov, R. Kappenberger, S. Wurmehl, B. Büchner, A. N. Yaresko, T. K. Kim, M. Hoesch, T. Wolf, and N. D. Zhigadlo, *Nature Physics* **12**, 311 (2016), Letter.
- [18] X.-P. Wang, P. Richard, Y.-B. Huang, H. Miao, L. Cevey, N. Xu, Y.-J. Sun, T. Qian, Y.-M. Xu, M. Shi, J.-P. Hu, X. Dai, and H. Ding, *Phys. Rev. B* **85**, 214518 (2012).
- [19] G. Derondeau, J. Braun, H. Ebert, and J. Minár, *Phys. Rev. B* **93**, 144513 (2016).
- [20] Z. P. Yin, K. Haule, and G. Kotliar, *Nature Physics* **7**, 294 (2011).
- [21] Y.-Z. Zhang, H. Lee, I. Opahle, H. O. Jeschke, and R. Valentí, *J. Phys. Chem. Sol.* **72**, 324 (2011).
- [22] J. Ferber, H. O. Jeschke, and R. Valentí, *Phys. Rev. Lett.* **109**, 236403 (2012).
- [23] N. Xu, P. Richard, A. van Roekeghem, P. Zhang, H. Miao, W.-L. Zhang, T. Qian, M. Ferrero, A. S. Sefat, S. Biermann, and H. Ding, *Phys. Rev. X* **3**, 011006 (2013).
- [24] Z. P. Yin, K. Haule, and G. Kotliar, *Nature Physics* **10**, 845 (2014).
- [25] M. Rotter, M. Tegel, D. Johrendt, I. Schellenberg, W. Hermes, and R. Pöttgen, *Phys. Rev. B* **78**, 020503 (2008).
- [26] M. Rotter, M. Tegel, and D. Johrendt, *Phys. Rev. Lett.* **101**, 107006 (2008).
- [27] K. Nakayama, T. Sato, P. Richard, Y.-M. Xu, T. Kawahara, K. Umezawa, T. Qian, M. Neupane, G. F. Chen, H. Ding, and T. Takahashi, *Phys. Rev. B* **83**, 020501 (2011).
- [28] N. Xu, P. Richard, X. Shi, A. van Roekeghem, T. Qian, E. Razzoli, E. Rienks, G.-F. Chen, E. Ieki, K. Nakayama, T. Sato, T. Takahashi, M. Shi, and H. Ding, *Phys. Rev. B* **88**, 220508 (2013).
- [29] C. Liu, T. Kondo, R. M. Fernandes, A. D. Palczewski, E. D. Mun, N. Ni, A. N. Thaler, A. Bostwick, E. Rotenberg, J. Schmalian, S. L. Bud’ko, P. C. Canfield, and

- A. Kaminski, *Nature Physics* **6**, 419 (2010).
- [30] J. Ferber, K. Foyevtsova, R. Valentí, and H. O. Jeschke, *Phys. Rev. B* **85**, 094505 (2012).
 - [31] M. Aichhorn, L. Pourovskii, V. Vildosola, M. Ferrero, O. Parcollet, T. Miyake, A. Georges, and S. Biermann, *Phys. Rev. B* **80**, 085101 (2009).
 - [32] Note, that the X point in our notation corresponds to the M point in the notation used by Werner *et al.*
 - [33] M. G. Kim, J. Lamsal, T. W. Heitmann, G. S. Tucker, D. K. Pratt, S. N. Khan, Y. B. Lee, A. Alam, A. Thaler, N. Ni, S. Ran, S. L. Bud'ko, K. J. Marty, M. D. Lumsden, P. C. Canfield, B. N. Harmon, D. D. Johnson, A. Kreyssig, R. J. McQueeney, and A. I. Goldman, *Phys. Rev. Lett.* **109**, 167003 (2012).
 - [34] Supplemental Material.
 - [35] V. N. Strocov, X. Wang, M. Shi, M. Kobayashi, J. Krempasky, C. Hess, T. Schmitt, and L. Patthey, *Synchrotron Radiat. News* **21**, 32 (2014).
 - [36] V. N. Strocov, M. Kobayashi, X. Wang, L. L. Lev, J. Krempasky, V. V. Rogalev, T. Schmitt, C. Cancellieri, and M. L. Reinle-Schmitt, *Synchrotron Radiat. News* **27**, 31 (2014).
 - [37] L. Moreschini, P.-H. Lin, C.-H. Lin, W. Ku, D. Innocenti, Y. J. Chang, A. L. Walter, K. S. Kim, V. Brouet, K.-W. Yeh, M.-K. Wu, E. Rotenberg, A. Bostwick, and M. Grioni, *Phys. Rev. Lett.* **112**, 087602 (2014).
 - [38] C.-H. Lin, T. Berlijn, L. Wang, C.-C. Lee, W.-G. Yin, and W. Ku, *Phys. Rev. Lett.* **107**, 257001 (2011).
 - [39] L. L. Lev, J. Krempaský, U. Staub, V. A. Rogalev, T. Schmitt, M. Shi, P. Blaha, A. S. Mishchenko, A. A. Veligzhanin, Y. V. Zubavichus, M. B. Tsetlin, H. Volfová, J. Braun, J. Minár, and V. N. Strocov, *Phys. Rev. Lett.* **114**, 237601 (2015).
 - [40] J. Braun and M. Donath, *Europhys. Lett.* **59**, 592 (2002).
 - [41] V. N. Strocov, *J. Electron. Spectrosc. Relat. Phenom.* **130**, 65 (2003).
 - [42] R. L. Kurtz, D. A. Browne, and G. J. Mankey, *J. Phys.: Cond. Mat.* **19**, 355001 (2007).
 - [43] H. Ebert, D. Ködderitzsch, and J. Minár, *Rep. Prog. Phys.* **74**, 096501 (2011).
 - [44] H. Ebert et al., *The Munich SPR-KKR package*, version 6.3, <http://olymp.cup.uni-muenchen.de/ak/eibert/SPRKKR>, 2012.
 - [45] G. Derondeau, S. Polesya, S. Mankovsky, H. Ebert, and J. Minár, *Phys. Rev. B* **90**, 184509 (2014).
 - [46] J. Minár, J. Braun, and H. Ebert, *J. Electron. Spectrosc. Relat. Phenom.* **189**, 129 (2013).
 - [47] J. Braun, K. Miyamoto, A. Kimura, T. Okuda, M. Donath, H. Ebert, and J. Minár, *New Journal of Physics* **16**, 015005 (2014).
 - [48] J. Minár, *J. Phys.: Cond. Mat.* **23**, 253201 (2011).

Acknowledgments

We thank V. Zabolotnyy and S. Borisenko for allowing us to use their experimental data. Special thanks goes to S. Biermann for discussions and ideas. We acknowledge financial support from the Deutsche Forschungsgemeinschaft DFG (projects FOR 1346) and from the Bundesministerium für Bildung und Forschung BMBF (project 05K13WMA). We further thank for the support from CENTEM PLUS (L01402). F. Bisti acknowledges the funding from the Swiss National Science Foundation under the grant agreement n.200021_146890 and European Community's Seventh Framework Programme (FP7/2007-2013) under the grant agreement n.290605 (PSI-FELLOW/COFUND).

Author contributions

G.D., V.N.S. and J.Mi. wrote the manuscript. F.B. V.A.R., M.K., T.S., J.Ma and V.N.S. performed the experiments and analyzed the data. G.D. performed the calculations. G.D., F.B., J.B., M.S., H.D., H.E., V.N.S. and J.Mi. participated at the discussions. J.Mi. supervised the theoretical part, V.N.S. supervised the experimental part.

Additional information

Supplemental Material accompanies this paper.

Competing financial interests: The authors declare no competing financial interests.

Supplemental Material for

Fermi surface and effective masses in photoemission response of the $(\text{Ba}_{1-x}\text{K}_x)\text{Fe}_2\text{As}_2$ superconductor

Gerald Derondeau,^{1,*} Federico Bisti,² Jürgen Braun,¹ Victor A. Rogalev,²
Masaki Kobayashi,^{2,3} Ming Shi,² Thorsten Schmitt,² Junzhang Ma,^{2,4,5}
Hong Ding,^{4,5} Hubert Ebert,¹ Vladimir N. Strocov,^{2,†} and Ján Minár^{1,6,‡}

¹*Department Chemie, Physikalische Chemie, Universität München,
Butenandtstr. 5-13, 81377 München, Germany*

²*Swiss Light Source, Paul Scherrer Institute, CH-5232 Villigen PSI, Switzerland*

³*Department of Applied Chemistry, School of Engineering,
University of Tokyo, 7-3-1 Hongo, Bunkyo-ku, Tokyo 113-8656, Japan*

⁴*Beijing National Laboratory for Condensed Matter Physics*

⁵*Institute of Physics, Chinese Academy of Sciences, Beijing 100190, China*

⁶*NewTechnologies-Research Center, University of West Bohemia, Pilsen, Czech Republic*

(Dated: June 26, 2022)

1. LIFSHITZ TRANSITION

A Lifshitz transition is characterized as a topological change of the Fermi surface.[1] For the iron pnictide superconductors this type of transition is of crucial importance as it is believed to mark the onset of superconductivity.[2–5] The K-doped $(\text{Ba}_{1-x}\text{K}_x)\text{Fe}_2\text{As}_2$ is a famous example for such a Lifshitz transition around the X point, leading to the discussed propeller topologies seen in ARPES experiments.[5–8] As known from experimental data [6–8] and the experiments performed within this work these topological features are already clearly visible for the optimally doped $(\text{Ba}_{0.6}\text{K}_{0.4})\text{Fe}_2\text{As}_2$. This is expected, following the argumentation that the Lifshitz transition suppresses the magnetic order due to a reduced nesting and thus induces superconductivity.[2, 9] However, the observed Lifshitz transition on the basis of the LDA was so far discussed only for high doping concentrations $x \approx 0.9$. [5, 10] It is also known that it is difficult to prepare homogeneous samples of over-doped $(\text{Ba}_{1-x}\text{K}_x)\text{Fe}_2\text{As}_2$ [5] which might explain discrepancies between various experiments about the onset of the Lifshitz transition.[6, 8, 10, 11] One remarkable and important paper from Khan and Johnson used the CPA to investigate the Lifshitz transition for $(\text{Ba}_{1-x}\text{K}_x)\text{Fe}_2\text{As}_2$ and they found a similar emergence of these propeller-like topologies for the heavily over-doped $(\text{Ba}_{0.1}\text{K}_{0.9})\text{Fe}_2\text{As}_2$. [5] However, with our new findings this result is now fully understandable. Using only a LDA based approach the relevant bands around X are still around 0.1 eV below the Fermi level (E_F). One can use over-doping with K in order to decrease E_F . The disadvantage of this approach is however that not only the relevant bands around X but the whole band structure is moved. Using a LDA+DMFT based approach one can see that correlation effects alter the electronic structure around X already for optimally doped $(\text{Ba}_{0.6}\text{K}_{0.4})\text{Fe}_2\text{As}_2$ so that the Lifshitz transition can emerge for lower doping concentration, in agreement with experiments.[6–8]

In order to show how this topology is affected by the correlation strength we show the corresponding BSF and FS in Fig. S1 for (A) LDA and LDA+DMFT with a varying on-site Coulomb interaction of (B) $U = 2.0$ eV, (C) $U = 3.0$ eV and (D) $U = 4.0$ eV with a constant exchange interaction $J = 0.9$ eV for Fe. Best agreement with experiment can be found for $U = 3.0$ eV as used and discussed in the main paper but it is also obvious that bands responsible for the Lifshitz transition are directly controlled by the Coulomb interaction U . Thus, we show that the origin of the important Lifshitz transition in $(\text{Ba}_{1-x}\text{K}_x)\text{Fe}_2\text{As}_2$ can be fully explained by correlation effects.

Still, it is also interesting to note that recent work on the ARPES spectra of the electron doped $\text{Ba}(\text{Fe}_{1-x}\text{Co}_x)_2\text{As}_2$ was successful using only a LDA approach.[12] The strength of correlation effects in the iron pnictides seem to vary with electron or hole doping.

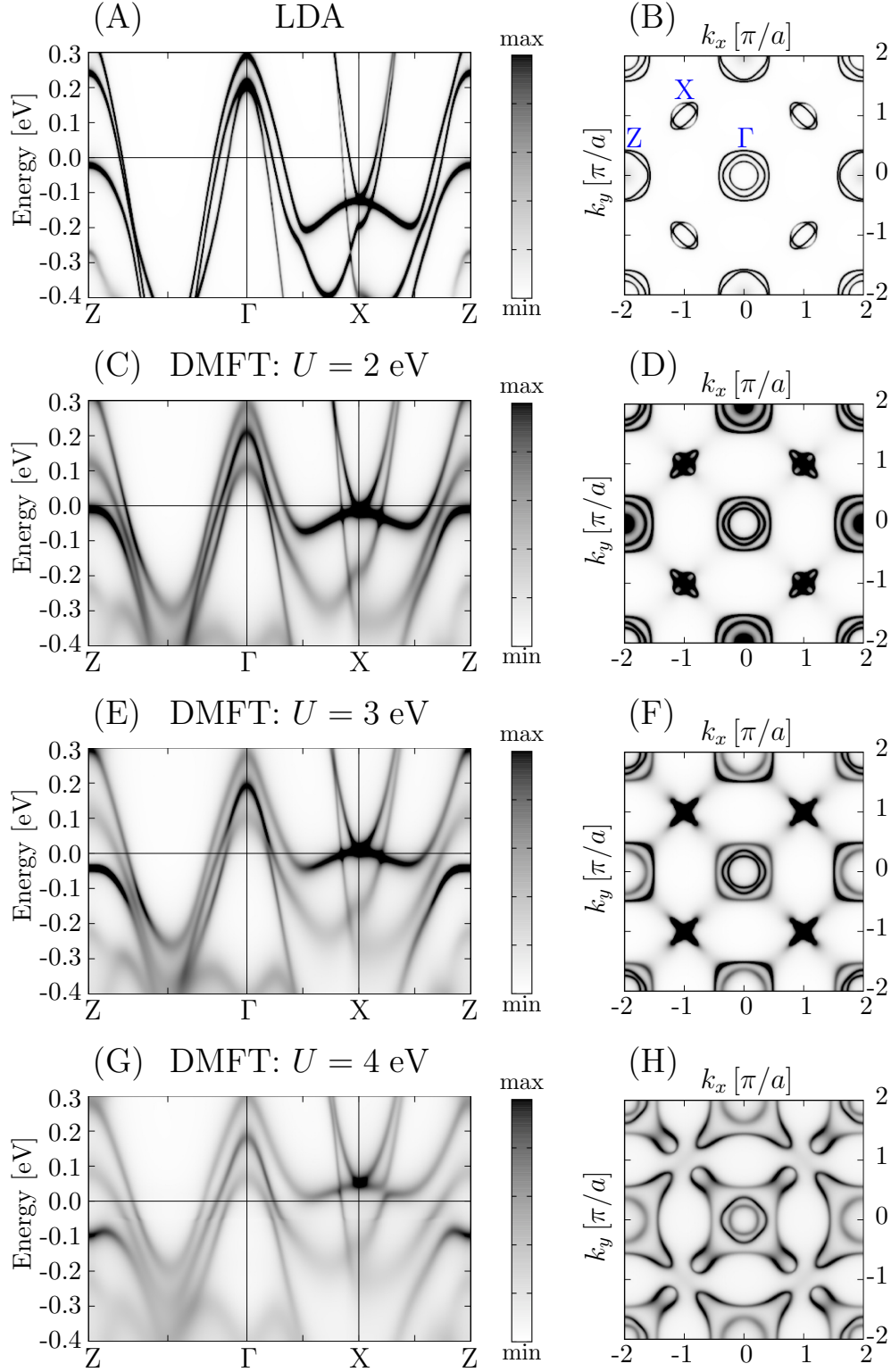


FIG. S1. (Color online) (A + B) BSF and FS of $(\text{Ba}_{0.6}\text{K}_{0.4})\text{Fe}_2\text{As}_2$ calculated on the basis of LDA. Corresponding BSF and FS of $(\text{Ba}_{0.6}\text{K}_{0.4})\text{Fe}_2\text{As}_2$ calculated on the basis of LDA+DMFT with (C + D) $U = 2.0$ eV, (E + F) $U = 3.0$ eV and (G + H) $U = 4.0$ eV for Fe ($J = 0.9$ eV).

2. EXTENDED FERMI SURFACE CUT

In correspondence to Fig. 3 of the main manuscript we present additionally extended Fermi surface cuts of $(\text{Ba}_{0.6}\text{K}_{0.4})\text{Fe}_2\text{As}_2$ for experimental data and theoretical calculations, respectively. Thus, Fig. S2 (A) shows the experimental data up to the second Brillouin zone and (B) the calculated Fermi surface cut up to the forth Brillouin zone, both images for p -polarized light and $h\nu = 430$ eV. This verifies that the alternating symmetry of the flower-like topology at $\bar{\Gamma}'$ compared to $\bar{\Gamma}$ is preserved over the whole k -space, in agreement with the data of Zabolotnyy *et al.* [6]. Interestingly, the flower-like topology changes a little bit for the third and forth Brillouin zone in Fig. S2 (B) which is connected to the k_z dispersion. Note, that the calculation is shown for a fixed photon energy of $h\nu = 430$ eV, thus, the effect of the k_z dispersion increases for higher Brillouin zones (see also the k_z scan in Fig. 4). In the experimental data of Fig. S2 (A) the value of k_z is corrected on the other hand. The blue square in (B) corresponds to the part of the Fermi surface shown in (A).

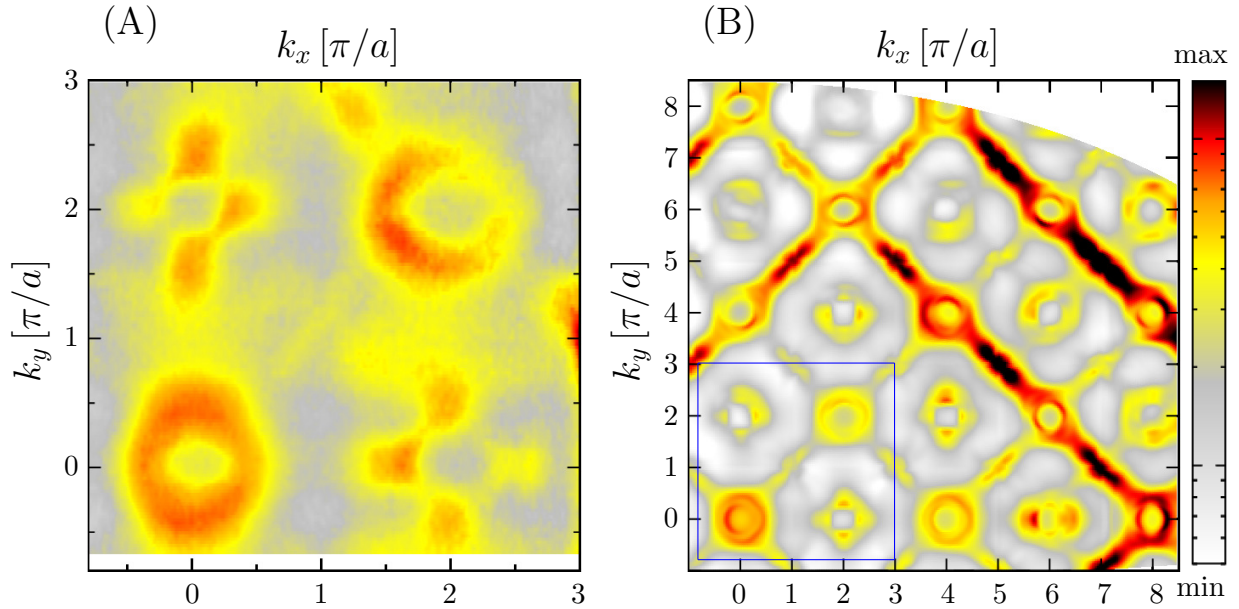


FIG. S2. Fermi surface cuts of $(\text{Ba}_{0.6}\text{K}_{0.4})\text{Fe}_2\text{As}_2$ with a fixed $h\nu = 430$ eV and for p -polarized light extending over several Brillouin zones. This is shown for (A) experimental data and (B) ARPES calculations using LDA+DMFT. The blue square in (B) corresponds to the part seen in (A).

3. DERIVED EFFECTIVE MASS ENHANCEMENT

In order to derive the mass enhancements shown in Tab. I the corresponding bands shown in Fig. S3 were used with the applied parabolic fits shown as solid green and red lines on top. For the BSF in Fig. S3 (A + B) and (E + F) the band dispersion can be fitted very reasonably by parabolic

functions. For the ARPES response however, final state effects, matrix element effects and surface effects alter the true band dispersion which results in bands showing more deviation from the perfect parabolic behavior. As discussed in the main paper, this is mainly due to final state effects which have a stronger impact the more pronounced the k_z dispersion of the corresponding bands is. Thus, the deviations from the perfect parabolic behavior are stronger in Fig. S3 (C + D) at the Γ point, compared to Fig. S3 (G + H) at the X point, because the bands at Γ have stronger 3D character whereas the band at X considered here is almost a 2D band. Furthermore, one should note that in the ARPES spectra the two outer bands around Γ are hardly distinguishable due to intensity loss connected to the ARPES response. As a technical detail, the calculations used an imaginary energy of 0.025 eV for the initial states and of 5.0 eV for the final states.

The resulting mass renormalization is shown in Fig. S4 (A - C) with the LDA bands from Fig. S3 (A) on top of the respective DMFT BSF and the DMFT ARPES response as dashed green and red lines. In addition, the DMFT bands of Fig. S3 (B) are shown on top of the ARPES spectra in Fig. S4 (D - E). This shows explicitly the deviation of the ARPES response from the true band dispersion derived from DMFT BSF. Consequently, the apparent mass enhancement seen in

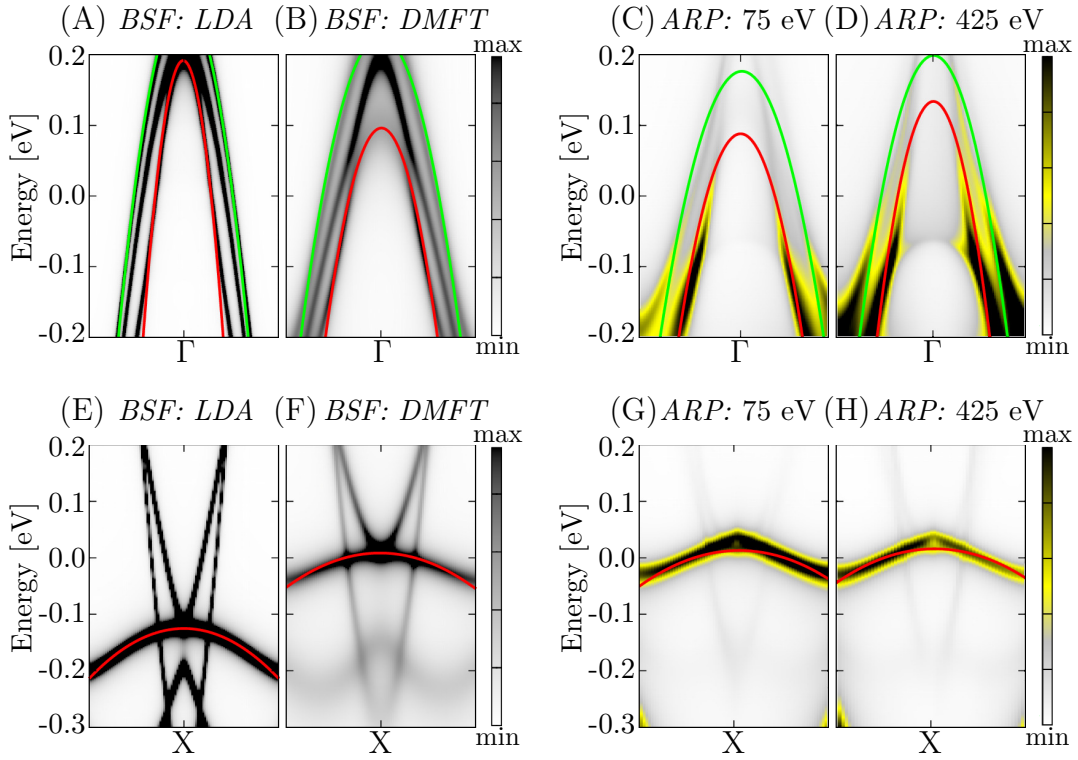


FIG. S3. Bands for which the mass enhancement is shown in Tab I. The solid red and green lines correspond to the applied parabolic plot fit. They are shown for (A - D) the Γ point having a strong k_z dispersion and for (E - H) the X point having a weak k_z dispersion. (A + E) BSF based on LDA, (B + F) BSF based on LDA+DMFT and (C + G) ARPES calculations based on DMFT for $h\nu = 75$ eV and (D + H) the same for $h\nu = 425$ eV.

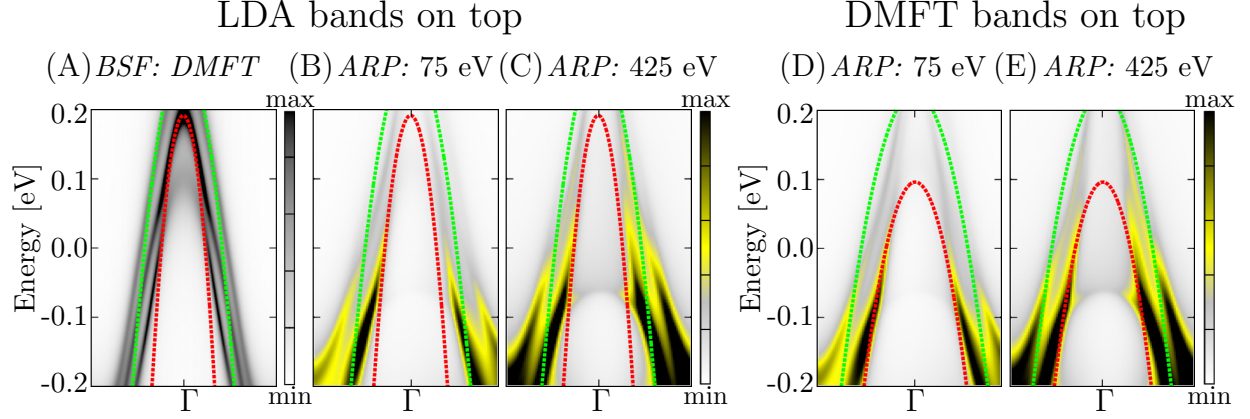


FIG. S4. (A - C) Band renormalization for BSF DMFT and the ARPES response with the LDA bands of Fig. S3 (A) on top. (D - E) The same ARPES spectra but with the DMFT bands of Fig. S3 (B) on top in order to show the effect only due to the ARPES response.

ARPES is affected by these ARPES response effects and thus it is not an intrinsic property of the quasiparticle valence band structure or spectral function. Why the ARPES response is affected by the k_z broadening Δk_z is depicted schematically in Fig. S5. As discussed in the main paper, Δk_z can be reduced by choosing a higher photon energy, although the resulting effects can be never fully avoided for 3D materials like the iron pnictides.

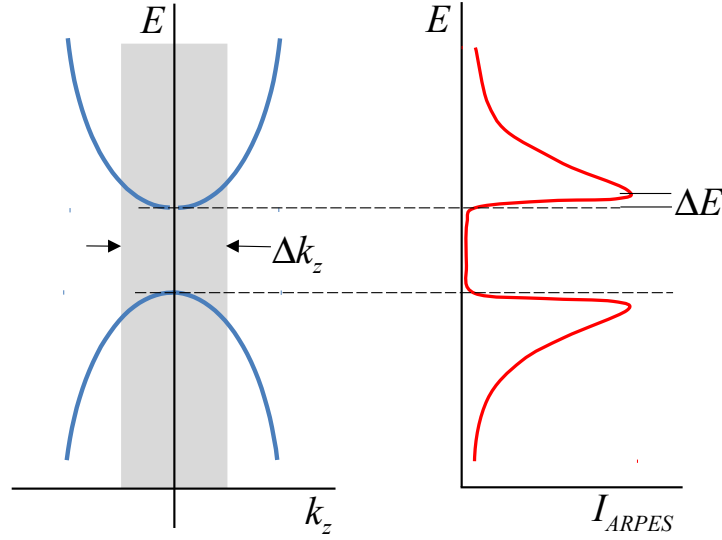


FIG. S5. Mechanism of the apparent mass enhancement (assuming a constant matrix element). The ARPES signal is formed by averaging of the valence band dispersion within the Δk_z broadening interval. Near the extremes of the k_z dispersion, this averaging results in asymmetry of the ARPES weight and shifting of the resulting spectral peak away from the extreme towards the band interior (for a more detailed picture including lifetime broadening of the valence states see Ref. [13]). Concerning its $k_{||}$ dependence of the ARPES spectra this shift causes an apparent reduction of the bandwidth and an increase of m^* .

* gerald.derondeau@cup.uni-muenchen.de

† vladimir.strocov@psi.ch

‡ jan.minar@cup.uni-muenchen.de

- [1] I. M. Lifshitz, Sov. Phys. J.E.T.P. **11**, 1130 (1960).
- [2] C. Liu, T. Kondo, R. M. Fernandes, A. D. Palczewski, E. D. Mun, N. Ni, A. N. Thaler, A. Bostwick, E. Rotenberg, J. Schmalian, S. L. Bud'ko, P. C. Canfield, and A. Kaminski, Nature Physics **6**, 419 (2010).
- [3] K. Matan, S. Ibuka, R. Morinaga, S. Chi, J. W. Lynn, A. D. Christianson, M. D. Lumsden, and T. J. Sato, Phys. Rev. B **82**, 054515 (2010).
- [4] C. Liu, A. D. Palczewski, R. S. Dhaka, T. Kondo, R. M. Fernandes, E. D. Mun, H. Hodovanets, A. N. Thaler, J. Schmalian, S. L. Bud'ko, P. C. Canfield, and A. Kaminski, Phys. Rev. B **84**, 020509 (2011).
- [5] S. N. Khan and D. D. Johnson, Phys. Rev. Lett. **112**, 156401 (2014).
- [6] V. B. Zabolotnyy, D. S. Inosov, D. V. Evtushinsky, A. Koitzsch, A. A. Kordyuk, G. L. Sun, J. T. Park, D. Haug, V. Hinkov, A. V. Boris, C. T. Lin, M. Knupfer, A. N. Yaresko, B. Büchner, A. Varykhalov, R. Follath, and S. V. Borisenko, Nature **457**, 569 (2009).
- [7] D. V. Evtushinsky, D. S. Inosov, V. B. Zabolotnyy, M. S. Viazovska, R. Khasanov, A. Amato, H.-H. Klauss, H. Luetkens, C. Niedermayer, G. L. Sun, V. Hinkov, C. T. Lin, A. Varykhalov, A. Koitzsch, M. Knupfer, B. Büchner, A. A. Kordyuk, and S. V. Borisenko, New Journal of Physics **11**, 055069 (2009).
- [8] D. V. Evtushinsky, A. A. Kordyuk, V. B. Zabolotnyy, D. S. Inosov, T. K. Kim, B. Büchner, H. Luo, Z. Wang, H.-H. Wen, G. Sun, C. Lin, and S. V. Borisenko, J. Phys. Soc. Japan **80**, 023710 (2011).
- [9] M. G. Kim, J. Lamsal, T. W. Heitmann, G. S. Tucker, D. K. Pratt, S. N. Khan, Y. B. Lee, A. Alam, A. Thaler, N. Ni, S. Ran, S. L. Bud'ko, K. J. Marty, M. D. Lumsden, P. C. Canfield, B. N. Harmon, D. D. Johnson, A. Kreyssig, R. J. McQueeney, and A. I. Goldman, Phys. Rev. Lett. **109**, 167003 (2012).
- [10] N. Xu, P. Richard, X. Shi, A. van Roekeghem, T. Qian, E. Razzoli, E. Rienks, G.-F. Chen, E. Ieki, K. Nakayama, T. Sato, T. Takahashi, M. Shi, and H. Ding, Phys. Rev. B **88**, 220508 (2013).
- [11] K. Nakayama, T. Sato, P. Richard, Y.-M. Xu, T. Kawahara, K. Umezawa, T. Qian, M. Neupane, G. F. Chen, H. Ding, and T. Takahashi, Phys. Rev. B **83**, 020501 (2011).
- [12] G. Derondeau, J. Braun, H. Ebert, and J. Minár, Phys. Rev. B **93**, 144513 (2016).
- [13] V. N. Strocov, J. Electron. Spectrosc. Relat. Phenom. **130**, 65 (2003).